

Observation of terahertz radiation coherently generated by acoustic waves

Michael R. Armstrong^{1*}, Evan J. Reed¹, Ki-Yong Kim², James H. Glowia², William M. Howard¹, Edwin L. Piner³ and John C. Roberts³

Over the past decade, pioneering and innovative experiments using subpicosecond lasers have demonstrated the generation and detection of acoustic and shock waves in materials with terahertz frequencies, the highest possible frequency acoustic waves^{1–5}. In addition to groundbreaking demonstrations of acoustic solitons, these experiments have led to new techniques for probing the structure of thin films^{6–8}. Terahertz-frequency electromagnetic radiation has been used in applications as diverse as molecular and material excitations^{9,10}, charge transfer^{11,12}, imaging¹³ and plasma dynamics¹⁴. However, at present, existing approaches to detect and measure the time dependence of terahertz-frequency strain waves in materials use direct optical probes—time-resolved interferometry or reflectometry^{2,15,16}. Piezoelectric-based strain gauges have been used in acoustic shock and strain wave experiments for decades, but the time resolution of such devices is limited to ~ 100 ps and slower, the timescale of electronic recording technology. We have recently predicted that terahertz-frequency acoustic waves can be detected by observing terahertz radiation emitted when the acoustic wave propagates past an interface between materials of differing piezoelectric coefficients^{17,18}. Here, we report the first experimental observation of this fundamentally new phenomenon and demonstrate that it can be used to probe structural properties of thin films.

As an acoustic wave traverses an interface between materials with differing piezoelectric response, polarization currents and concurrent radiation are predicted to be generated at the boundary. These currents radiate on the timescale of the strain changes¹⁷. For acoustic waves with characteristic frequencies of terahertz (corresponding to picosecond timescales), terahertz radiation is emitted. This phenomenon bears a close resemblance to the so-called transition radiation phenomenon that occurs when a charged particle propagates past an interface between two dielectric materials, generating polarization currents and radiation from the interface. It is distinct from a narrowband, coherent terahertz emission mechanism that has been predicted to occur when a planar shock wave propagates through an ionic crystal^{19–21}. When the interface is flat and some propagation properties of the strain wave are known, the time dependence of the strain can be computed from the time dependence of the radiated electric field. This enables the observation of ultrafast strain profiles in regions of a material not accessible to active probes such as those used in interferometry- or reflectometry-based methods^{2,22–24}. This acoustic transition radiation phenomenon has been predicted theoretically¹⁷, but not yet observed experimentally. Some experimental evidence exists for other forms of electromagnetic radiation that may

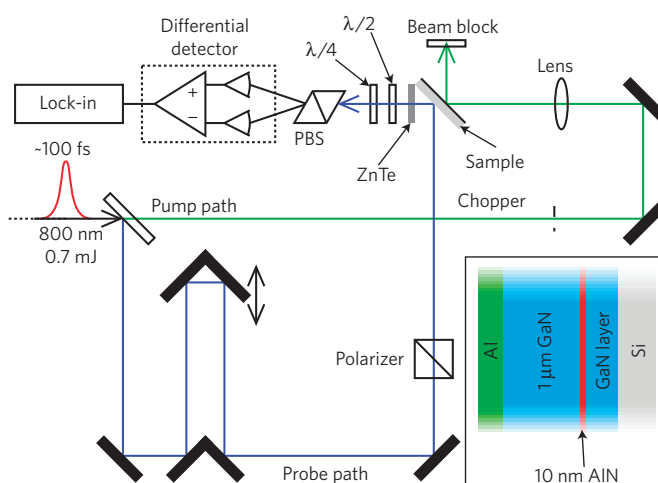


Figure 1 | Schematic diagram of the experimental set-up. PBS is a polarizing beam separator; $\lambda/2$ and $\lambda/4$ are a half waveplate and quarter waveplate, respectively. The inset shows a cross-section of the sample. The pump is incident on the Al-coated side of the sample.

exhibit some correlation with acoustic processes^{23,25}. Here, we describe experimental results demonstrating acoustically generated terahertz radiation that is coherently related to the strain-wave time dependence through a well-understood physical mechanism. We emphasize that, in contrast to commonly used terahertz generation^{10,11,26,27}, we report observations of radiation generated by the terahertz-frequency acoustic wave; that is, the signal is not conversion of an ultrashort optical pulse to terahertz radiation through the optical response of the sample.

The experimental scheme is shown in Fig. 1. In the present work, boundaries between regions of differing piezoelectric response are formed by a submicrometre thick layer of aluminium on gallium nitride, and a layer of AlN embedded in the GaN, as shown in the inset to Fig. 1. Piezoelectric wurtzite crystal structure GaN is oriented with its c axis perpendicular to the sample surface. Terahertz radiation is generated when strain waves pass through the Al–GaN boundary and through the embedded AlN layer and the radiation is detected using conventional electro-optic sampling^{26,27}.

The acoustic wave is generated by focusing an ultrashort (~ 100 fs) optical pulse onto the Al layer, which heats the metal within ~ 3.5 ps through a depth of about 50 nm (ref. 28). Thermal expansion generates a wave with maximum strain of the order of -0.01 corresponding to pressures of the order of 1 GPa. Although the form of the acoustic wave is dependent primarily on material

¹CMEELS Directorate, Lawrence Livermore National Laboratory, Livermore, California 94550, USA, ²CINT, Los Alamos National Laboratory, Los Alamos, New Mexico 87545, USA, ³Nitronex Corp., 2305 Presidential Dr., Durham, North Carolina 27703, USA. *e-mail: armstrong30@llnl.gov.

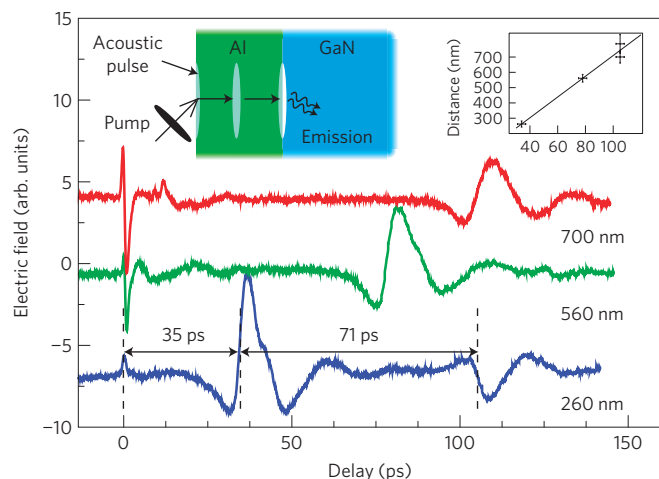


Figure 2 | Electric field from Al-GaN interface versus time. The plots are labelled by Al layer thickness. Dispersion in the shape of the pulse is primarily due to polycrystalline effects in the Al layer. An acoustic reflection in the Al layer radiates around 105 ps in the 260 nm Al-coated sample. The transit times are labelled for the 260 nm trace. Inset: Layer thickness versus transit time in picoseconds. A fit to the transit distance versus time gives a sound speed of 6.7 km s^{-1} compared to the Al bulk sound speed 6.4 km s^{-1} .

properties that have longer characteristic times than the pump pulse, the acoustic pulse generated at the Al surface is well synchronized with the pump.

Figure 2 shows the detected electric field for various thicknesses of Al coated on GaN. Around $t = 0$ when the pump arrives at the Al surface, a fast terahertz signal is observed, which is probably generated through the nonlinear optical response of the sample and/or photocurrent generation at the metal-air interface²⁶. This signal is not believed to be related to acoustic emission but provides a convenient marker for $t = 0$. At later times, the electric field exhibits slower variation corresponding to the acoustic pulse arrival at the Al-GaN interface. The arrival times at the interface vary linearly with the thickness of the Al layer in each sample (see Fig. 2, inset), demonstrating a linear correlation between the time of emission and the acoustic transit time with a fitted acoustic velocity of $6.7 \text{ km s}^{-1} \pm 6\%$ (compare to 6.4 km s^{-1} sound speed in Al). Surface probe techniques²⁹ indicate that broadening of the pulse with increasing Al thickness primarily results from the distribution in sound speed as a function of grain orientation in the polycrystalline Al film. The $\sim 1 \text{ mm}$ pump diameter generates a strain wave that is significantly larger than the characteristic size of the crystallites in the Al film. We observe the duration of the fast rise in the acoustic profile to vary between 2 ps for thin Al layers ($< 100 \text{ nm}$) to approximately 5 ps after propagation through 700 nm of Al. Data taken with a lower pump power (for a single Al thickness) exhibited electric field profiles with rise times equivalent to the higher power to within 1 ps. This suggests that polycrystalline acoustic speed dispersion is a more significant effect than nonlinear effects at the strains generated in these experiments.

The term 'nanoseismology'²³ has been proposed to characterize the study of thin-film nanostructures using high-frequency acoustic waves. Such studies so far have used optical techniques to observe reflected strain waves at surfaces. Acoustic transition radiation enables a new approach to materials characterization for piezoelectric structures. Structural details of a heterostructure may be determined by injecting a well-characterized acoustic profile and measuring the emitted electric field to determine the locations of boundaries between materials in the heterostructure. Figure 3 shows the electric field versus time for three different samples with different Al layer thicknesses. A signal is generated when the wave

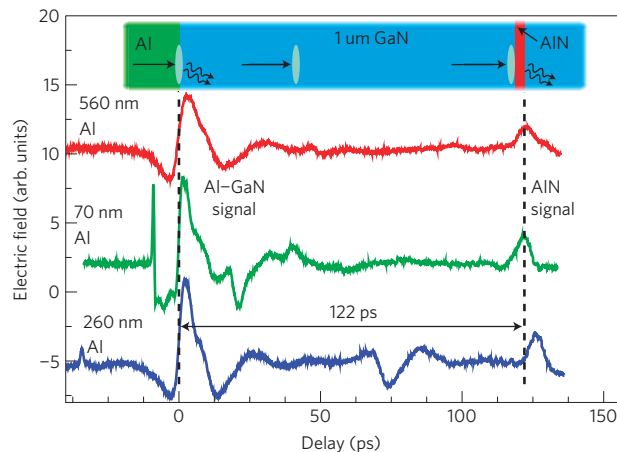


Figure 3 | Electric field versus time for several Al thicknesses. The peak at $\sim 70 \text{ ps}$ in the 260 nm trace is an acoustic echo in Al. A time shift of the AlN signal in the 260 nm Al case suggests variations in the GaN layer thickness across the sample.

crosses the AlN layer because the piezoelectric coefficients for GaN and AlN differ. The transit time through the GaN layer is consistent at $\sim 122 \text{ ps}$ (GaN speed of sound: $8.00 \pm 0.02 \text{ km s}^{-1}$; ref. 5). We attribute variations in the transit time to variation in the GaN thickness across the wafer. The transit delay between the Al-GaN signal and the AlN signal is consistent enough to establish that the observed peak results from the acoustic wave traversing the AlN layer. As the single-crystal GaN layer does not exhibit polycrystalline dispersion, scatter in the AlN signal probably indicates variation in the thickness of the $1 \mu\text{m}$ GaN layer, which smears out the AlN peak. Acoustic transition radiation may enable potentially nanometre-scale resolution in a non-destructive measurement for comprehensive, rapid, online process control for thin-film growth.

Figure 4 shows an expanded version of data from the sample coated with 260 nm of Al along with the stress estimated from the electric field distribution through an approach related to that of Reed *et al.*¹⁷. The recovered stress is qualitatively consistent with the expected form of an acoustic pulse excited by an ultrafast pump from a free surface^{3,8}. For comparison, an ALE3D simulation of the stress assuming uniform illumination at 50 mJ cm^{-2} fluence is also shown. Thermal expansion of the Al layer from pump illumination launches two counter-propagating compression pulses, the first towards the Al-GaN boundary and the second towards the Al-free surface (at the Al-air boundary). The compression pulses have a timescale of roughly the spatial depth of the thermal deposition divided by the sound speed. The second compression pulse is reflected from the Al-free surface with a 180° phase shift, resulting (with the first compression pulse) in a composite wave comprising an initial compression followed by a faster expansion to a tensile state (over the timescale of the thermal deposition) followed by a slower compression. The resulting acoustic profile is characteristic of an acoustic pulse generated by ultrafast laser excitation at a metal-free surface^{4,8}.

Figure 4 also shows the first reflection from the Al-GaN boundary and the Al-free surface, after the pulse has made two more passes through the Al layer. The reflected pulse exhibits a 180° total phase shift with each double pass, resulting from reflection from GaN (a higher impedance material than Al resulting in no sign change) and the free surface, which gives a 180° phase shift (a sign change). Although the fastest electric field rise times measured were 2–3 ps (implying $< 0.5 \text{ THz}$ emission), the stress recovery exhibits lower acoustic bandwidth. For instance, the fast, expansive portion of the stress in the 260 nm Al sample has a 5 ps rise (compared with a $\sim 3 \text{ ps}$ rise in the electric field), consistent with

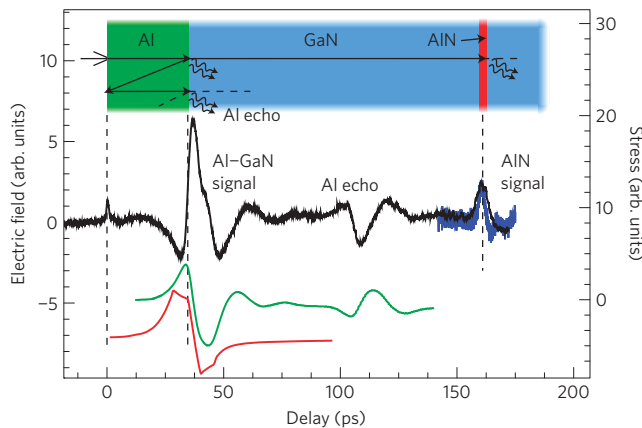


Figure 4 | Electric field versus time for the 260 nm Al sample (top black trace). After the stress wave initially encounters the Al–GaN interface, an acoustic echo is detected, corresponding to the acoustic wave traversing the Al layer two more times. The echo has the opposite sign compared with the initial Al–GaN signal. Signal from the AlN layer is detected at a time delay consistent with the thickness of the top GaN layer, 1 μm . The blue curve shows a time-shifted 1 ps finite difference of the Al–GaN signal overlaid on the AlN signal. The narrower width of the finite difference of the Al–GaN signal suggests roughness in the adjacent GaN layer. Also depicted is the stress calculated from the electric field (middle green trace) compared to the stress from a simulation of the acoustic profile (red, offset from the recovered stress) having the same qualitative form.

acoustic measurements in related systems using interferometry^{2,29}. The simulated stress is similar qualitatively to the measured stress. We expect some variation from the recovered stress due to polycrystalline dispersion in the experiment, which is not present in the simulation (the simulation models a single crystal of Al).

Finally, the signal from the 10 nm layer of AlN is expected to take the form of a finite difference of the single interface signal over the acoustic transit time through the AlN layer (1 ps for a sound speed of 10 km s^{-1} in AlN). For comparison, a 1 ps finite difference of the single interface (Al–GaN) signal is shown in Fig. 4 superposed with the AlN signal. The finite difference and the AlN signal have the same qualitative form, but the AlN signal has a larger pulse width, which we attribute to variation of the GaN thickness over the pump diameter.

We note that recovery of transient stress on nanometre length scales inside a sample is challenging using an active probe method such as interferometry, which requires a metallic interface to achieve nanometre spatial resolution, an otherwise optically transparent sample, and is adversely affected by acoustically modulated index variation in the sample, particularly for large-amplitude acoustic waves. Although sample preparation necessarily involves the fabrication of piezoelectric interfaces and requires the sample to be transmissive at terahertz frequencies, acoustically generated terahertz radiation may be detected independently from an arbitrary number of sufficiently spaced interfaces along the acoustic wave trajectory. In addition, owing to the longer wavelength of terahertz radiation, emission is less susceptible to optical inhomogeneity and pressure-induced index of refraction variation in the sample due to the wave. In particular, for the GaN heterostructure of Fig. 4, it would be challenging to obtain the stress profile at the 10 nm AlN layer using an active optical probe or X-ray diffraction. The Al and Si surfaces of this sample prevent optical probes with photon energy above the Si bandgap from reaching the AlN layer.

Terahertz detection techniques have been demonstrated for frequencies well above 10 THz, but we expect the properties of the strained material and strain wave to limit the bandwidth generated.

In these experiments, the bandwidth of input strain pulses limits the bandwidth of the detected radiation. Our earlier theoretical work suggests that higher frequencies of 3 THz and potentially above may be detectable for higher pressure stress waves¹⁷.

Methods

The GaN sample is epitaxially grown on an atomically flat silicon (111) substrate by Nitronex, Inc., comprising layers grown by metal organic chemical vapour deposition³⁰ of (from free space to the Si substrate) 1 μm GaN, 10 nm of AlN, >400 nm of GaN, a proprietary transition layer and the Si substrate. Each Al layer was sputter-coated over a 4 mm diameter, with the thicknesses measured by Dektak, giving thicknesses of 700 ± 40 nm, 560 ± 30 nm and 260 ± 20 nm. The error in the thickness measurement was dominated by wafer warp. The Al surface is assumed to be flat with respect to the Al–GaN interface, with thickness variation of less than 10 nm, corresponding to less than 2 ps variation in acoustic transit time.

To obtain coupling between radiation modes and polarization currents that are along the c axis (that is, perpendicular to the sample surface), the sample is tilted 45° off the optic axis. We directly detect the strain-induced electric field through electro-optic sampling with a 3-mm-thick (110) ZnTe crystal in a pump–probe scheme with differential lock-in detection^{10,26,27} using a low-energy, ~ 100 -fs-duration, 800 nm probe pulse that is reflected from the back of the Si substrate, which has been polished to optical surface quality.

The 3-mm-thick ZnTe crystal provides >1 THz detection bandwidth²⁷, but does not exhibit strong terahertz reflections, simplifying the data analysis. Strong terahertz sample reflections are not evident in the data (see Fig. 2, where ZnTe reflections would be observed at ~ 60 ps and sample reflections at 10 ps) with the maximum reflection amplitude observed <20%. The ZnTe crystal is 2–3 mm from the sample along the probe beam. The field is sampled every 33 fs and the data are averaged over a moving window of 20 samples, reducing the time resolution to ~ 700 fs. The experiment is non-destructive (the pump fluence is below the damage threshold), and all experiments are multiple shot averages at half the pulse repetition rate of the laser, 500 Hz, with a 300 ms lock-in integration time. The pump pulse has 800 nm wavelength, ~ 100 fs duration, ~ 700 μJ energy and 1.1 mm diameter (full-width at half-maximum intensity).

We recover the time-dependent stress from the electric field distribution using a method related to that described in Reed *et al.*¹⁷, which includes the effects of a Gaussian beam-width distribution in stress. For the frequencies of interest, the electric field from the radiating source can be treated as a point time-dependent polarization with electric field at point \mathbf{r} given by,

$$E(\mathbf{r}, t) = -\hat{r} \times \hat{z} \times \hat{r} \frac{\dot{p}(t-r/c)}{c^2 r} + [3\hat{r}(\hat{r} \cdot \hat{z}) - \hat{z} \hat{z}] \left(\frac{\dot{p}(t-r/c)}{cr^2} + \frac{p(t-r/c)}{r^3} \right) \quad (1)$$

where $\dot{p}(t) = \pi \sigma_{zz}(t) d c_s \ell^2$ is the current generated by the wave of Gaussian beam-width of radius ℓ and centre stress $\sigma_{zz}(t)$. The piezoelectric coefficient of GaN is d and the acoustic wave speed is c_s . In equation (1), the polarization of the current is in the \hat{z} direction and hats denote unit vectors. Equation (1) is solved for the time dependence of the stress $\sigma_{zz}(t)$ given by the electric field using a finite-difference scheme. We take $r = 6.5$ mm corresponding to the approximate optical path length between the source and detector because the far-field term in equation (1) dominates under the conditions of the experiments (equation (1) applies in a uniform medium and therefore represents an approximation to sample geometry used here). Although determination of the time dependence of the stress is relatively straightforward, quantitative calculation of the stress magnitude is made challenging by the difficulties of calibrating the detection apparatus and complicated field and experiment geometry. Our initial attempts to determine the magnitude of the electric fields that we observed vary by a factor of three depending on the calibration method used. We expect the accuracy of the calibration to improve with further work.

Received 14 August 2008; accepted 12 February 2009; published online 15 March 2009

References

- Hao, H. Y. & Maris, H. J. Experiments with acoustic solitons in crystalline solids. *Phys. Rev. B* **64**, 064302 (2001).
- Gahagan, K. T. *et al.* Measurement of shock wave rise times in metal thin films. *Phys. Rev. Lett.* **85**, 3205–3208 (2000).
- Muskens, O. L. & Dijkhuis, J. I. High amplitude, ultrashort, longitudinal strain solitons in sapphire. *Phys. Rev. Lett.* **89**, 285504 (2002).
- Muskens, O. L., Akimov, A. V. & Dijkhuis, J. I. Coherent interactions of terahertz strain solitons and electronic two-level systems in photoexcited ruby. *Phys. Rev. Lett.* **92**, 035503 (2004).
- Wu, S. *et al.* Femtosecond optical generation and detection of coherent acoustic phonons in GaN single crystals. *Phys. Rev. B* **76**, 085210 (2007).

6. Thomsen, C., Grahn, H. T., Maris, H. J. & Tauc, J. Surface generation and detection of phonons by picosecond light-pulses. *Phys. Rev. B* **34**, 4129–4138 (1986).
7. Maris, H. J. Picosecond ultrasonics. *Sci. Am.* **278**, 86–89 (1998).
8. Saito, T., Matsuda, O. & Wright, O. B. Picosecond acoustic phonon pulse generation in nickel and chromium. *Phys. Rev. B* **67**, 205421 (2003).
9. Grischkowsky, D., Keiding, S., Vanexter, M. & Fattinger, C. Far-infrared time-domain spectroscopy with terahertz beams of dielectrics and semiconductors. *J. Opt. Soc. Am. B* **7**, 2006–2015 (1990).
10. Ferguson, B. & Zhang, X. C. Materials for terahertz science and technology. *Nature Mater.* **1**, 26–33 (2002).
11. Beard, M. C., Turner, G. M. & Schmuttenmaer, C. A. Terahertz spectroscopy. *J. Phys. Chem. B* **106**, 7146–7159 (2002).
12. Groot, M. L. *et al.* Coherent infrared emission from myoglobin crystals: An electric field measurement. *Proc. Natl Acad. Sci. USA* **99**, 1323–1328 (2002).
13. Chan, W. L., Deibel, J. & Mittleman, D. M. Imaging with terahertz radiation. *Rep. Prog. Phys.* **70**, 1325–1379 (2007).
14. Kim, K. Y. *et al.* Measurements of terahertz electrical conductivity of intense laser-heated dense aluminum plasmas. *Phys. Rev. Lett.* **100**, 135002 (2008).
15. Evans, R. *et al.* Time- and space-resolved optical probing of femtosecond-laser-driven shock waves in aluminum. *Phys. Rev. Lett.* **77**, 3359–3362 (1996).
16. Bolme, C. A., McGrane, S. D., Moore, D. S. & Funk, D. J. Single shot measurements of laser driven shock waves using ultrafast dynamic ellipsometry. *J. Appl. Phys.* **102**, 033513 (2007).
17. Reed, E. J., Armstrong, M. R., Kim, K. Y. & Glowia, J. H. Atomic-scale time and space resolution of THz frequency acoustic waves. *Phys. Rev. Lett.* **101**, 014302 (2008).
18. Reed, E. J. *et al.* Terahertz radiation from shocked materials. *Mat. Today* **10**, 44–50 (2007).
19. Reed, E. J., Soljagic, M., Gee, R. & Joannopoulos, J. D. Molecular dynamics simulations of coherent optical photon emission from shock waves in crystals. *Phys. Rev. B* **75**, 174302 (2007).
20. Reed, E. J., Soljagic, M., Gee, R. & Joannopoulos, J. D. Coherent optical photons from shock waves in crystals. *Phys. Rev. Lett.* **96**, 013904 (2006).
21. Reed, E. J., Soljagic, M. & Joannopoulos, J. D. Maxwell equation simulations of coherent optical photon emission from shock waves in crystals. *Phys. Rev. E* **75**, 056611 (2007).
22. Geindre, J. P. *et al.* Frequency-domain interferometer for measuring the phase and amplitude of a femtosecond pulse probing a laser-produced plasma. *Opt. Lett.* **19**, 1997–1999 (1994).
23. Stanton, C. J. *et al.* Coherent phonons, nanoseismology and THz radiation in InGaN/GaN heterostructures. *Superlatt. Microstruct.* **34**, 525–529 (2003).
24. Sun, C. K., Liang, J. C. & Yu, X. Y. Coherent acoustic phonon oscillations in semiconductor multiple quantum wells with piezoelectric fields. *Phys. Rev. Lett.* **84**, 179–182 (2000).
25. Hayes, B. Detonation electric effect. *J. Appl. Phys.* **38**, 507–511 (1967).
26. Mittleman, D. (ed.) *Sensing with Terahertz Radiation* (Springer, 2003).
27. Gallot, G. & Grischkowsky, D. Electro-optic detection of terahertz radiation. *J. Opt. Soc. Am. B* **16**, 1204–1212 (1999).
28. Siwick, B. J., Dwyer, J. R., Jordan, R. E. & Miller, R. J. D. An atomic-level view of melting using femtosecond electron diffraction. *Science* **302**, 1382–1385 (2003).
29. Slayton, R. M. & Nelson, K. A. Picosecond acoustic transmission measurements. I. Transient grating generation and detection of acoustic responses in thin metal films. *J. Chem. Phys.* **120**, 3908–3918 (2004).
30. Weeks, W. T., Piner, E. L., Gehrke, T. & Linthicum, K. J. Patent No. 6,617,060 (2003).

Acknowledgements

We thank R. Averitt, C. Bolme, P. Celliers, R. Chau, R. Collins, J. Eggert, L. Fried, D. Funk, D. Hicks, N. Holmes, D. Moore, J. Nguyen, R. Patterson and C. Tarver for helpful discussions. This work was supported by the LLNL LDRD program, the LANL CINT user program, and carried out in part under the auspices of the US Department of Energy by Lawrence Livermore National Laboratory under Contract DE-AC52-07NA27344.

Author contributions

M.R.A.: experiments, data analysis; E.J.R.: theory, simulations, data analysis; K.Y.K.: experiments, data analysis; J.H.G.: facility, applications; W.M.H.: simulations; E.L.P. and J.C.R.: sample fabrication.

Additional information

Reprints and permissions information is available online at <http://npg.nature.com/reprintsandpermissions>. Correspondence and requests for materials should be addressed to M.R.A.